



UNIVERSITY
OF TRENTO

DEPARTMENT OF INFORMATION AND COMMUNICATION TECHNOLOGY

38050 Povo – Trento (Italy), Via Sommarive 14
<http://www.dit.unitn.it>

ELECTROMAGNETIC DETECTION OF DIELECTRIC SCATTERERS USING
PHASELESS SYNTHETIC AND REAL DATA AND THE MEMETIC
ALGORITHM

Salvatore Corsi, Andrea Massa, Matteo Pastorino, and Andrea
Randazzo

August 2004

Technical Report DIT-04-066

ELECTROMAGNETIC DETECTION OF DIELECTRIC SCATTERERS USING PHASELESS SYNTHETIC AND REAL DATA AND THE MEMETIC ALGORITHM

S. Caorsi,¹ A. Massa,² M. Pastorino,³ and A. Randazzo³

¹Department of Electronics

University of Pavia

Via Ferrata 1, 27100 Pavia, ITALY.

Phone: + 39 0382505661 Fax: +39 0382422583 e-mail: caorsi@ele.unipv.it

³ Department of Information and Communication Technology

University of Trento

Via Sommarive 14, I-38050 Trento, ITALY.

Phone: +39 0461882057 Fax: +39 0461881696 e-mail: andrea.massa@ing.unitn.it

³ Department of Biophysical and Electronic Engineering

University of Genoa

Via Opera Pia 11A, 16145, Genova, ITALY.

Phone: +39 010352242 Fax: +39 0103532245 e-mail: pastorino@dibe.unige.it

Abstract - Phaseless data are used to evaluate the application of an electromagnetic inverse-scattering-based procedure for the detection of cylindrical inhomogeneities, which are schematized as multilayer infinite dielectric cylinders with elliptic cross sections. The electromagnetic inverse problem is recast as a global optimization problem and iteratively solved by an efficient memetic algorithm, which combines deterministic and stochastic concepts. Moreover, a recursive analytical procedure is used for the forward scattering computation. The possibility of localizing and reconstructing the scatterers by using phaseless input data, which would greatly simplify the design of the imaging apparatus, is evaluated both with reference to synthetically produced data and by means of experimental data obtained by a microwave tomograph.

Keywords: Electromagnetic imaging, inverse scattering, elliptic cylinders, genetic algorithms

I. INTRODUCTION

The detection of pipes, tunnels and other cylindrical structures (for example those encountered in the inspection of archeological sites) by means of electromagnetic waves has been recently addressed in several works [1]-[7]. The need for detecting dielectric structures suggests the exploitation of inverse-scattering-based electromagnetic techniques, which can be considered as an extension of the now popular ground penetrating radar. Moreover, the detection of inhomogeneities is a challenging topic in several other applications, including nondestructive evaluation and testing in civil engineering and medical imaging [8]-[10].

It is well known that the inverse scattering problem resulting from the electromagnetic modeling of the detection configuration is ill-posed and highly nonlinear [11]. Great care must be exercised in the definition of the problem unknown, in the parametrization required by the integral equations/Green's function operators, and in the choice of the functional to be minimized (usually, the inverse scattering formulation is recast as an optimization problem). Several techniques have been devised in recent years. Although the best results were so far obtained by using iterative procedures (see, for example, [12]-[15] and the references therein), the use of stochastic global optimization procedures (e.g., genetic and evolutionary algorithms [16]) has also been recently considered [17]-[20] and allowed by the tremendous increasing of the computer powers. In fact, the main drawback of these procedures is represented by the computational load, since the convergence is usually very slow when they are implemented on serial computer. The greatest advantage of these techniques, widely discussed in several review papers [21]-[23], is related to the potential ability of finding the global minimum of a given functional, relatively independently of the structure of the functional itself (convexity, differentiability, etc.). In the author's opinion, another significant characteristic of these procedures, which is very important for the purpose of solving inverse scattering problems in real applications, is represented by the possibility of including a priori information into the model in a very simple way.

In most of the previously mentioned applications there is also the need for the design of simple, fast, and economic detection apparatus. To this end, a schematic representation of the cylindrical structures to be detected is often considered, with a reduction of the parametrization dimensions. Usually, the distribution of the internal electric field is not required (e.g., in nondestructive evaluation and subsurface detection). However, this distribution is not known and for strong scatterers it cannot be approximated by the known distribution of the incident field [24]. In addition, the need for the measurement of the complex scattered field at the acquisition probes requires a reference channel and a synchronous detection in order to obtain phase data. Although at

microwaves and lower frequencies the measurement of the phase is not a technical problem, the possibility of using phaseless input data can notably simplify the design of the imaging apparatus. A lot of work has been recently made concerning the advantages associated with techniques based on amplitude-only data for several applications, including measurement and diagnoses of antennas, source reconstruction, dielectric permittivity estimation, and radar signal processing [25]-[30].

In the present paper the dielectric cylinders under test are represented by multilayer elliptic cylinders resorting to an efficient analytical model in order to compute the forward scattering needed for the developed iterative procedure. Firstly, an assessment of the multimodality of the functional to be minimized is presented. Successively, dielectric reconstructions are performed starting by phaseless input scattering data. In particular, the functional resulting from the inverse scattering formulation is minimized by applying a memetic algorithm, which has been found to be effective in a number of applications [31]-[32]. The most important feature of the approach is represented by the combination of the capability of the genetic algorithm in reaching the global minimum with the efficiency of deterministic local search methods. To the best of our knowledge, it is the first time that a memetic algorithm is applied to an inverse scattering problem with reduced information content of data (phaseless data).

In the results section, the procedure is tested by considering both synthetic and experimental scattering data. In the first case, exact analytical values are used as input data with reference to a configuration previously considered in the literature and usually solved starting by complex data (amplitude and phase). In the second case, the input data are constituted by real data obtained in an anechoic chamber by the French team of K. Belkebir and co-workers by means of a microwave illumination/measurement system.

II. MATHEMATICAL FORMULATION

A layered infinite cylinder, composed by L confocal elliptical layers, is illuminated by a set of incident electric fields TM-polarized (i.e., with the electric field vector polarized along the cylindrical axis). For the numerical simulations the incident fields are produced by a set of line current sources, so that

$$\Psi_{inc}(\mathbf{x}, \mathbf{x}_s) = -\frac{jI}{\eta} H_0^{(2)}(k|\mathbf{x} - \mathbf{x}_s|) \quad (1)$$

where $\Psi_{inc}(\mathbf{x})$ is the z -component of the incident field vector, \mathbf{x}_s , $s = 1, \dots, S$, is the source position, $H_0^{(2)}$ is the second-order Hankel function of zero-th order, I is the amplitude of the line current, and k and η are the wavenumber and the intrinsic impedance of the propagation medium, respectively. The scattered electric field can be collected in a set of M points \mathbf{y}_m , $m = 1, \dots, M$, where the probes are to be located. The scattered field can be expressed as:

$$\begin{aligned} \Psi_{scatt}(\mathbf{y}) = & \sum_{m=0}^{+\infty} e_m^{L+1} M c_m^{(4)}(q_{L+1}, u) c e_m(q_{L+1}, v) + \\ & + \sum_{m=0}^{+\infty} o_m^{L+1} M s_m^{(4)}(q_{L+1}, u) s e_m(q_{L+1}, v) \end{aligned} \quad (2)$$

where a series expansion in terms of Mathieu functions in elliptic coordinates ($\mathbf{y} = u\mathbf{u} + v\mathbf{v}$) has been used [33]. In equation (2), $M c_m^{(4)}$, $M s_m^{(4)}$, $c e_m$ and $s e_m$ denote the fourth-order radial and angular Mathieu functions, respectively, whereas e_m^{L+1} and o_m^{L+1} are unknown coefficients to be determined. Finally, $q_{L+1} = (kd/2)^2$, being d the half focal distance of the elliptical cross section.

The z -component of the internal total field vector is given by [33]:

$$\begin{aligned} \Psi_{tot}^i(\mathbf{y}) = & \sum_{m=0}^{+\infty} [e_{m,1}^i M c_m^{(1)}(q_i, u) + e_{m,2}^i M c_m^{(2)}(q_i, u)] c e_m(q_i, v) + \\ & + \sum_{m=0}^{+\infty} [o_{m,1}^i M s_m^{(1)}(q_i, u) + o_{m,2}^i M s_m^{(2)}(q_i, u)] s e_m(q_i, v) \end{aligned} \quad (3)$$

where $M c_m^{(1)}$, $M s_m^{(2)}$, $c e_m$ and $s e_m$ indicate odd and even radial Mathieu functions; q_i is given by $q_i = (k_i d/2)^2$, where k_i is the wavenumber in the i -th layer; finally, $e_{m,1}^i$, $e_{m,2}^i$, $o_{m,1}^i$ and $o_{m,2}^i$ denote the unknown coefficients.

Let us measure the phaseless values of the total electric field at the measurement points. After constructing the data set $\{\Xi_m^s, m = 1, \dots, M, s = 1, \dots, S\}$, the functional to be minimized is expressed as:

$$F(\xi_k) = \frac{\sum_{s=1}^S \sum_{m=1}^M |\Psi_{tot}^{(k)}(\mathbf{y}_m, \mathbf{x}_s, \xi_k) - \Xi_m^s|^2}{\sum_{s=1}^S \sum_{m=1}^M \Xi_m^s{}^2} \quad (4)$$

where $\Psi_{tot}^{(k)}(\mathbf{y}_m, \mathbf{x}_s, \xi_k)$ is the total electric field computed at point \mathbf{y}_m when the source is at point \mathbf{x}_s and the scatterer is a cylinder characterized by the parameters constituting the array ξ_k , which is defined as:

$$\xi_k = (x_0^{(k)}, y_0^{(k)}, a_1^{(k)}, \dots, a_L^{(k)}, \epsilon_1^{(k)}, \dots, \epsilon_L^{(k)}, d^{(k)}) \quad (5)$$

The values of $\Psi_{tot}^{(k)}(\mathbf{y}_m, \mathbf{x}_s, \xi_k)$ are analytically computed as the sum of the known incident field and the scattered electric field given by equation (1), in which the unknown coefficients of the series expansion are efficiently computed by the recursive procedure described in [34]. Since $F(\xi_k)$ is iteratively minimized by applying the memetic algorithm, in equations (4) and (5), k represents the iteration number. We used here a single frequency processing; however, the functional $F(\xi_k)$ can be easily extended to the multifrequency case.

III. APPLICATION OF THE MEMETIC ALGORITHM

The memetic algorithm combines, at each iteration, a local search and a stochastic minimization. When it was introduced, the algorithm was aimed at "emulating the process of exchange of ideas among people." However, from a computational point of view, it belongs to the class of evolutionary methods and can be considered as a hybrid genetic algorithm. Essentially, the use of a local search is aimed at increasing the convergence velocity, whereas the same genetic operators of the genetic algorithm are applied to escape from local minima. The method combines the advantages of both stochastic and deterministic minimization procedures and usually requires a limited population. We used a real code implementation for the *memes* on which the genetic operators act. Detailed discussions concerning implementation, capabilities and limitations of the memetic algorithm can be found in [30]-[32] and in the references therein. Concerning the implementation used in the present paper, Figure 1 provides a flow chart of the algorithm. In particular, since the memetic algorithm is a population-based method, the first operation is the creation of an initial set of trial solutions, which is randomly performed by using the function $Rand(x,y)$, which returns random values uniformly distributed. $g(i)$ denotes the i -th element of the initial population of the algorithm, whose dimension is indicated with M . Any element of the population is used as a starting point for a local search algorithm. As a result of this first operation, a set of M local minima is obtained. When the starting set has been defined, the genetic operators

are applied on the population. The three considered operators are indicated by $select(g_1, g_2)$, $crossover(g_1, g_2)$, and $mutate(g_1, g_2)$, where g_1 and g_2 are two individuals of the population. In particular, the selection operator, denoted by $select(g_1, g_2)$, chooses two elements of the population for reproduction. The reproduction consists of two operations. First, the selected individuals are mated by using the single-point cross over function [32] ($crossover(g_1, g_2)$) in order to create two new arrays with a probability p_c . Later, the mutation operator ($mutate(g_1, g_2)$) is applied with a probability p_m . The obtained elements are then optimized by the local search procedure. The *Replacement* block performs the substitution of the old population with the new individuals created by the previous operators. In particular, all new elements are copied into the population except the worst element, which is replaced with the best one of the old population (*elitism* operator). In Figure 1, K_{max} and F_{th} denote the maximum number of iterations and the threshold for the cost function, respectively. The iterative algorithm terminates when the cost function $F(\xi)$ reaches a value below F_{th} or when the number of generations exceeds K_{max} .

IV. NUMERICAL RESULTS

In the first example, we consider the reconstruction of a buried elliptic cylinder with the measurement points arranged in a borehole configuration (the geometry is shown in the inset of Figure 2). Synthetic data are used as input data and, according to the assumptions made in [7], in which a similar configuration has been assumed, the effect of the interface is neglected. The purpose of this first example is the evaluation of the impact of phaseless data on the functional to be minimized. In particular, Figure 2 shows the functional to be minimized in the case of complete data and phaseless data (equation (4)). The dielectric cylinder has a cross section of elliptic shape, which is centered at point $x_0 = -0.173\lambda$, $y_0 = -0.865\lambda$, being λ the wavelength of the incident wave. The semi major axis of the ellipse is 0.26λ , The semi-focal distance is $d = 0.245\lambda$. The dielectric permittivity of the void cylinder is ϵ_0 and the background medium is characterized by $\epsilon_b = 12\epsilon_0$ and $\mu_b = \mu_0$.

The scattered data are collected at a set of 13 measurement points, which are uniformly distributed along a probing line at points $x_m = 0.865\lambda$, $y_m = -(m-1) \cdot 0.173\lambda$, $m = 1, \dots, 13$. The incident wave is produced by a line source located at $x_s = -0.865\lambda$, $y_s = -1.04\lambda$.

As can be seen from Figure 2, in the phaseless case one more local minimum is present and the other local minimum is much deeper (clearly, the functional related to the complex input data is multimodal, too). Figures 3(a)-(d) show pictorial representations of the functional $F(\xi)$ computed for different values of x_0 , y_0 and ϵ_r . It is evident that $F(\xi)$, in the phaseless case (Figures 3 (b) and

3(d)), is much more irregular than the corresponding functional for complete data (Figure 3(a) and 3(c)). As expected, phase data, when available, are very important, since they represent additional information of the inverse scattering experiment. Nevertheless, the application of an efficient global optimization algorithm may allow the correct reconstruction of the unknown target even in the phaseless case, in which, as counterpart, a far simpler measurement apparatus can be used.

In particular, by using the memetic algorithm, the following reconstructions have been obtained. Figure 4 shows the behavior of the cost function (equation (4)) for three elements of the population. After the first iteration of the memetic algorithm, the convergence threshold ($F(\xi) \leq F_{th} = 10^{-5}$) is reached. In Figure 4, "CG_{ij}" denotes the value of the functional $F(\xi)$ for the j -th element of the population, whereas "MA" indicates the value of $F(\xi)$ for the best element of the population at the i -th iteration of the memetic algorithm. The initialization phase is denoted by $i = 0$. Between two iterations of the memetic algorithm (in the present case, between the initialization and the first iteration), the plots are related to the local search. The small rhomb denotes the optimum element. It is evident that the local search is trapped in local minima, whereas the application of the genetic operators (after the local search) enables to escape from the local minima and explore a different region of the solution space, allowing the convergence of the process. However, unlike the classic genetic algorithm, in the memetic algorithm the genetic operators are applied few times and the main search process is performed by the local search procedure. As a result, the memetic algorithm is faster than the genetic algorithm.

Analogously, Figure 5 gives the values of the reconstructed dielectric permittivity. In particular, at the convergence, the relative error is less than 5 %. The parameters used for the memetic algorithm are listed in Table I. In order to provide a deeper assessment of the behavior of the memetic algorithm at the various iterations and, in particular, to better evaluate the capabilities of the method to escape from local minima, Figures 6 shows the "movements" of the coordinate of center of the elliptic cross section during the minimization phases, including the local search and the application of the genetic operators. In particular, in Figure 6, the continuous lines denote the "movements" of the trial solutions during the initialization phase, whereas the dashed lines denote "movements" during the first iteration of the memetic algorithm. Moreover, the black triangles indicate the starting points and the white triangles indicate the arrival points of the local search. Again, the small rhomb denotes the optimum element. From figures 5 and 6, it is quite evident the capabilities of the method to avoid local minima, whereas the usually applied iterative inversion procedures can be trapped there if care is not exercised in the choice of the initial trial solution. The "jumps" in the solution space are particularly evident in Figure 5, which also confirm the local-minimum nature of the trial solutions of the memetic algorithm. See, for example, the two

trajectories on the right part of the figure: A trial solution of the initialization phase reaches a local minimum at about $x = 0.36\lambda$, $y_s = -1.52\lambda$. The same local minimum is reached, during the first iteration of the memetic algorithm, by another trial solution starting from a different point. Finally, as can be clearly seen from Figures 5 and 6, the memetic approach is able to reach the global minimum even with starting solutions very far from the correct data (e.g., in Figure 5, the relative dielectric permittivity is equal to about 40 for the starting solution). In the authors' opinion, this feature of the approach can be quite important in the light of practical applications.

A preliminary result concerning a two-layer elliptic cylinder is reported in Figure 7, which gives the final images of the reconstructed elliptic cross sections at the various iterations of the memetic algorithm, corresponding to the best elements constructed during the minimization process. The parameters of the two-layer model are the following: the cross-section center is $x_0 = -0.173\lambda$, $y_0 = -0.865\lambda$; the semi major axes of the ellipses defining the external boundaries of the two layers are equal to 0.26λ and 0.295λ ; the semi-focal distance is $d = 0.245\lambda$; the relative dielectric permittivities are 1.0 (inner layer) and 5.0 (external layer). All the other parameters of the configuration are the same as those used in the previous example. The final solution is reached after 5 iterations of the memetic algorithm (which has been run with the same parameters listed in Table I). In particular, the behavior of the cost function for the best element of the iterative optimization process is reported in Figure 8. As can be seen, at iterations $k = 1$ and $k = 2$, the same local minimum is reached, for which the same cross section is obtained in the final image (Figure 7). After iteration $k = 1$, in fact, the genetic operators produced a new optimum solution very near to the optimum solution at the end of the local search of iteration $k = 1$. However, the excellent capabilities of the approach in escaping from local minima are clearly shown in the last two iterations.

V. EXPERIMENTAL RESULTS

The proposed inversion procedure has also been tested by considering real input data. In particular, the measurement data have been obtained by K. Belkebir, M. Saillard and co-workers at the Institut Fresnel, UMR-CNRS, Marseille, France, by using a tomographic imaging configuration [35]-[37]. The experiment has been carried out in a circular configuration, i.e. the antennas (emitting and receiving antennas) are located on circles surrounding the unknown object. Actually, the transmitting antenna is fixed and the object is rotated, which is equivalent to rotate the emitting antenna. Double-ridged horn antennas are used (ARA DRG118A of dimensions 14.30×24.13 cm²). The distance between the center of the experimental setup and the emitting antenna is $r_s =$

72.135 cm, whereas the distance between the center of the experimental setup and the receiving antenna is $r_r = 76.135$ cm.

The electric field is measured at 49 points located on a circular line of radius r_r . A multiview approach is used (36 views). Furthermore, the data are collected using 4 frequencies, varying from 4 to 16 GHz. The object to be reconstructed is an infinite cylinder with circular cross section and relative dielectric permittivity $\epsilon_r=3.0$; the radius is 0.015 m and the center is located at point (0.0, 0.03) m. In the present paper, in order to test the reconstruction procedure, only one view and one frequency (4 GHz) are used and the threshold has been fixed to $F_{th} = 10^{-2}$. In particular, the procedure described in Section II is applied to reconstruct the coordinates of the center of the circular cross section and the semi minor axis (*smina*).

Results are reported in Figures 9-12. In particular, Figure 9 shows the behavior of the functional $F(\xi)$ at various iteration steps and Figure 10 gives the errors (normalized to the wavelength) in the reconstruction of the center of the cylinder cross-section. As can be seen, after four iterations of the memetic algorithm, the cylinder is located very well although the starting point (corresponding to the best individual) is rather distant from the exact one and the input data are noisy amplitude-only data. Moreover, Figure 11 shows the reconstructed values of the normalized semi minor axis, which, at convergence, reaches with a good approximation the exact value of the dielectric cylinder used for the experiment.

Finally, Figure 12 reports the trajectories of each trial solution during the entire minimization process in the planes x -*smina* and y -*smina*, confirming the capability of the approach in escaping from local minima.

VI. CONCLUSIONS

The phaseless reconstruction of cylindrical inhomogeneities has been explored in this paper. A global optimization method has been applied, which is based on a memetic algorithm, which combines a series of local searches with the use of genetic operators. The unknown cylinders are schematized by multilayer elliptic cylinders, for which the forward problem, at the various iterations, has been analytically solved by a recursive procedure. Synthetic data are used for the reconstruction of cylinders in a borehole configuration. Moreover, the procedure has been validated by real scattering data obtained in a tomographic arrangement. Although the functional to be minimized, in the phaseless data, results to be highly multimodal, locations and shapes of the unknown cylinders have been reconstructed quite accurately, due to the ability of the memetic algorithm to escape from local minima.

ACKNOWLEDGMENT

The authors wish to thank Prof. Kamal Belkebir for having very kindly allowed the use of the measurement data obtained by its research group at the Institut Fresnel, UMR-CNRS, Marseille Cedex, France. The authors wish also to express their gratitude to Dr. Johan Wettergreen for having provided the subroutines for the computation of the Mathieu functions.

REFERENCES

- [1] C. Dourthe, Ch. Pichot, J. Y. Dauvignac, and J. Cariou, "Inversion algorithm and measurement system for microwave tomography of buried object," *Radio Sci.*, vol. 35, pp. 1097-1108, Sept.-Oct. 2000.
- [2] Z. Q. Zhang and Q. H. Liu, "Two nonlinear inverse methods for electromagnetic induction measurements," *IEEE Trans. Geosci. Remote Sensing*, vol. 39, pp. 1331-1339, 2001.
- [3] I. T. Rekanos and T. D. Tsiboukis, "A finite element-based technique for microwave imaging of two-dimensional objects," *IEEE Trans. Instrum. Meas.*, vol. 49, pp. 234-239, 2000.
- [4] S. Caorsi, G. L. Gragnani and M. Pastorino, "Numerical electromagnetic inverse-scattering solutions for two-dimensional infinite dielectric cylinders buried in a lossy half-space," *IEEE Trans. Microwave Theory Tech.*, vol. 41, pp. 352-356, Feb. 1993.
- [5] L. Chommeloux, Ch. Pichot, and J.-C. Bolomey, "Electromagnetic modeling for microwave imaging of cylindrical buried inhomogeneities," *IEEE Trans. Microwave Theory Tech.*, vol. 34, pp. 1064-1076, Oct. 1986.
- [6] S. Caorsi, A. Massa, and M. Pastorino, "A computational technique based on a real-coded genetic algorithm for microwave imaging purposes," *IEEE Trans. Geosc. Remote Sensing*, Special Issue on "Computational Wave Issues in Remote Sensing, Imaging and Target Identification," vol. 38, pp. 1697-1708, 2000.
- [7] K. A. Michalski, "Electromagnetic imaging of elliptical-cylindrical conductors and tunnels using a differential evolution algorithm," *Microwave and Opt. Technol. Lett.* 28 (2001) 164-167.
- [8] S. J. Lockwood and H. Lee, "Pulse-echo microwave imaging for NDE of civil structures: Image reconstruction, enhancement, and object recognition," *Int. J. Imaging Systems Technol.*, vol. 8, pp. 407-412, 1997.

- [9] D. Hughes and R. Zoughi, "A method for evaluating the dielectric properties of composites using a combined embedded modulated scattering and near-field microwave nondestructive testing technique," Proc. 18th IEEE Instrum. Meas. Technol. Conf., Budapest, Hungary, pp. 1882-1886, 2001.
- [10] S. K. Moore, "Better breast cancer detection," *IEEE Spectrum*, May issue, pp. 50-55, 2001.
- [11] M. Bertero and P. Boccacci, *Introduction to Inverse Problems in Imaging*, IOP, Bristol, UK, 1998.
- [12] W. C. Chew and Y. M. Wang, "Reconstruction of two-dimensional permittivity distribution using the distorted Born iterative method," *IEEE Trans. Med. Imaging*, vol. 9, pp. 218-225, 1990.
- [13] R. E. Kleinman and P. M. van den Berg, "Two-dimensional location and shape reconstruction," *Radio Sci.*, vol. 29, pp. 1157-1169, 1994.
- [14] A. G. Tijhuis, K. Belkebir, A. C. S. Litman, and B. de Hon, "Theoretical and computational aspects of 2-D inverse profiling," *IEEE Trans. Geosci. Remote Sensing*, vol. 39, pp. 1316-1330, 2001.
- [15] K. Meyer, K. J. Langenberg, and R. Schneider, "Microwave imaging of defects in solids," Proc. 21st Annual Review of Progress in Quantitative NDE, Snowmass Village, Colorado, USA, 1994.
- [16] D. Golberg, "Genetic and evolutionary algorithms come of age" *Comm. of the ACM*, vol. 37, pp. 113-119, 1994.
- [17] Z. P. Qian and W. Hong, "Image reconstruction of conducting cylinder based on FD-MEI and genetic algorithm," Proc. IEEE APS Int. Symp., vol. 2, pp. 718-721, 1998.
- [18] C. C. Chiu and P. T. Liu, "Image reconstruction of a perfectly conducting cylinder by the genetic algorithm," *IEE Proc. Microwave Antennas Propag.*, vol. 143, 1996.
- [19] S. Caorsi, A. Massa, and M. Pastorino, "A microwave imaging procedure for NDT identification of a crack based on a genetic algorithm for nondestructive testing," *IEEE Transactions on Antennas Propagat.*, vol. 49, no. 12, Dec. 2001.
- [20] S. Kent and T. Gunel, "Dielectric permittivity estimation of cylindrical objects using genetic algorithm," *J. Microwave Power and Electromagn. Energy*, vol. 32, pp. 109-113, 1997.
- [21] R. L. Haupt, "An introduction to genetic algorithms for electromagnetics," *IEEE Antennas Propagat. Mag.*, 37, 2, 7-15, 1995.
- [22] D. S. Weile and E. Michielssen, "Genetic algorithm optimization applied to electromagnetics: a review," *IEEE Trans. Antennas Propagat.*, vol. 45, pp. 343-353, March 1997.

- [23] J. M. Johnson and Y. Rahmat-Samii, "Genetic algorithms in engineering electromagnetics," *IEEE Antennas Propagat. Mag.*, vol. 39, pp. 7-25, Apr. 1997.
- [24] M. Slaney, A. C. Kak, and L. E. Larsen, "Limitation of imaging with first-order diffraction tomography," *IEEE Trans. Microwave Theory Tech.*, vol. 32, pp. 860-873, 1984.
- [25] R. G. Yaccarino, Y. Rahmat-Samii, "Phaseless bi-polar planar near-field measurements and diagnostics of array antennas," *IEEE Trans. Antennas Propagat.*, vol. 47, pp. 574-583, March 1999.
- [26] F. Las-Heras and T. K. Sarkar, "A direct optimization approach for source reconstruction and NF-FF transformation using amplitude-only data," *IEEE Trans. Antennas Propagat.*, vol. 50, pp. 500-510, April 2002.
- [27] M. F. Akay, S. N. Kharkovsky, and U. C. Hasar, "An automated amplitudes-only measurement system for permittivity determination using free-space method," Proc. 18th IEEE Instrum. Meas. Technol. Conf. (IMTC 2001), vol. 1, pp. 503-506, 2001.
- [28] M. Lambert and D. Lesselier, "Binary-constrained inversion of a buried cylindrical obstacle from complete and phaseless magnetic fields," *Inverse Problems*, vol. 16, pp. 563-576, 2000.
- [28] C. D. Reeve and J. F. Wombwell, "Novel space-integrating acousto-optic correlator: amplitude and phase information from intensity only measurements," *IEE Proceedings (Radar, Sonar and Navigation)*, vol. 136, pp. 185-190, Aug. 1989.
- [29] R. G. Yaccarino and Y. Rahmat-Samii, "A comparison of conventional and phaseless planar near-field antenna measurements: the effect of probe position errors," Proc. IEEE Int. Conf. on Phased Array Systems and Technology, pp. 525-528, 2000.
- [30] P. Moscato, "On evolution, search, optimization, genetic algorithms and martial arts towards memetic algorithms," Tech. Rep. Caltech Concurrent Computation Program, Report. 826, California Institute of Technology, Pasadena, California, USA, 1989.
- [31] P. Moscato and M. G. Norman, "A 'memetic' approach for the traveling salesman problem. Implementation of a computational ecology for combinatorial optimization on message-passing systems," in: M. Valero, E. Onate, M. Jane, J. L. Larriba and B. Suarez (Eds.), *Parallel Computing and Transputer Applications*, IOS Press, Amsterdam, pp. 187-194, 1992.
- [32] P. Merz and B. Freisleben, "Fitness landscape analysis and memetic algorithms for the quadratic assignment problem," *IEEE Trans. Evolutionary Computation*, vol. 4, pp. 337-352, Nov. 2000.
- [33] J. J. Bowman, T. B. A. Senior, and P. L. E. Uslenghi, *Electromagnetic and Acoustic Scattering by Simple Shapes*. Amsterdam, The Netherlands: North-Holland, 1969.

- [34] S. Caorsi, M. Pastorino and M. Raffetto, "Electromagnetic scattering by a multilayer elliptic cylinder: series solution in terms of Mathieu functions," *IEEE Trans. Antennas Propagat.*, vol. 45, pp. 926-935, June 1997.
- [35] K. Belkebir, "Reconstruction of two-dimensional complex permittivity distributions from real data," Proc. Workshop on Microwave Imaging Methods and Techniques, 20-th European Microwave Conf., Paris, 2000.
- [36] K. Belkebir and M. Saillard, "Special section: Testing inversion algorithms against experimental data," *Inverse Problems*, vol. 17, pp. 1565-1571, 2001.
- [37] K. Belkebir, S. Bonnard, F. Pezin, P. Sabouroux, M. Saillard, "Validation of 2D inverse scattering algorithms from multi-frequency experimental data," *J. Electromagnetic Waves Appl.*, vol. 14, 1637-1667, 2000.

FIGURE AND TABLE CAPTIONS

Figure 1 – Flow chart of the memetic algorithm.

Figure 2 – The functional $F(\xi)$ in the case of complete and phaseless data (equation (4)) computed along the y -coordinate of the cross-section center.

Figure 3 – The functional $F(\xi)$ computed for different values of the cross-section center and of the relative dielectric permittivity. (a)(c) Complete data (amplitude and phase). (b)(d) Phaseless data.

Figure 4 – The functional $F(\xi)$ computed for three elements of the population.

Figure 5 – Reconstructed values of the dielectric permittivity of the cylinder versus the iteration number.

Figure 6 – Trajectories of the individuals of the population of the memetic algorithm in the x - y -plane (coordinates of the cross-section center).

Figure 7 – Reconstruction of a two-layer elliptic cylinder. Cross section of the cylinder at the various iterations of the memetic algorithm (best elements of the population).

Figure 8 – Reconstruction of a two-layer elliptic cylinder. Behavior of the functional $F(\xi)$ for the best element of the population.

Figure 9 – The functional $F(\xi)$ computed for three elements of the population versus the iteration number. Real scattering data.

Figure 10 – Errors on the reconstruction of the cross-section center. The errors are normalized to the wavelength, λ .

Figure 11 – Reconstructed values of the semi minor axis ($smina$) at the various iterations of the memetic algorithm.

Figure 12 – Trajectories of the individuals of the population of the memetic algorithm in the two planes (a) x - $smina$ (semi minor axis) and (b) y - $smina$.

Table I - Parameters of the memetic algorithm for the numerical simulation.

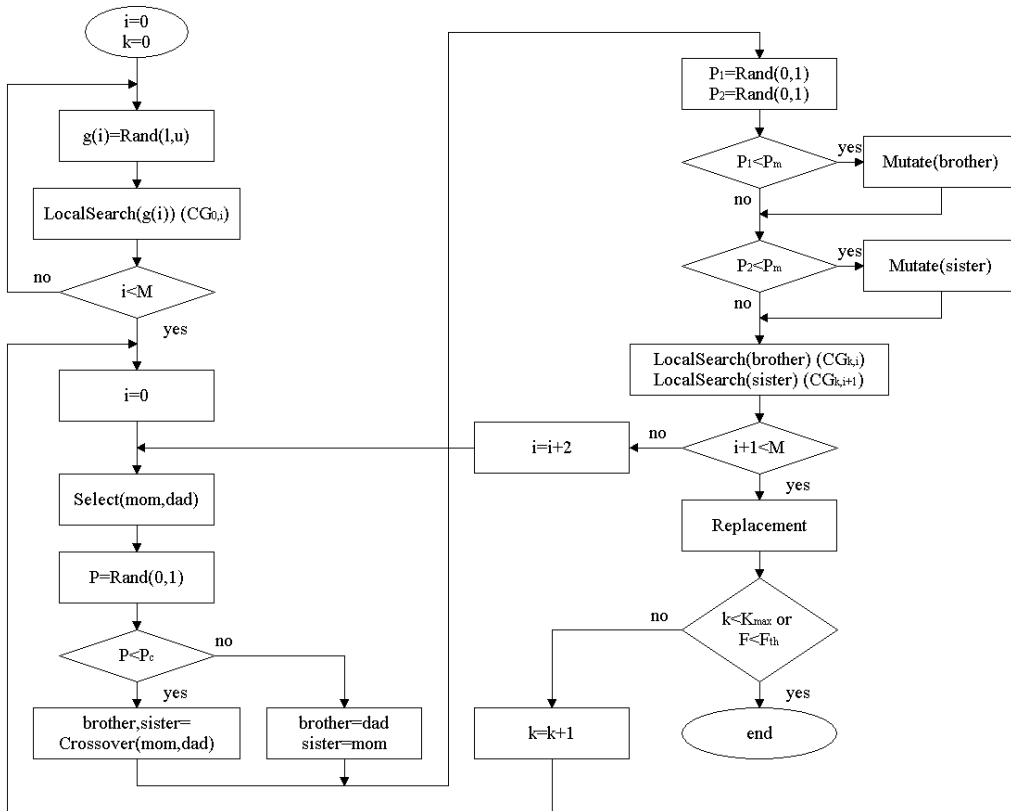


Figure 1

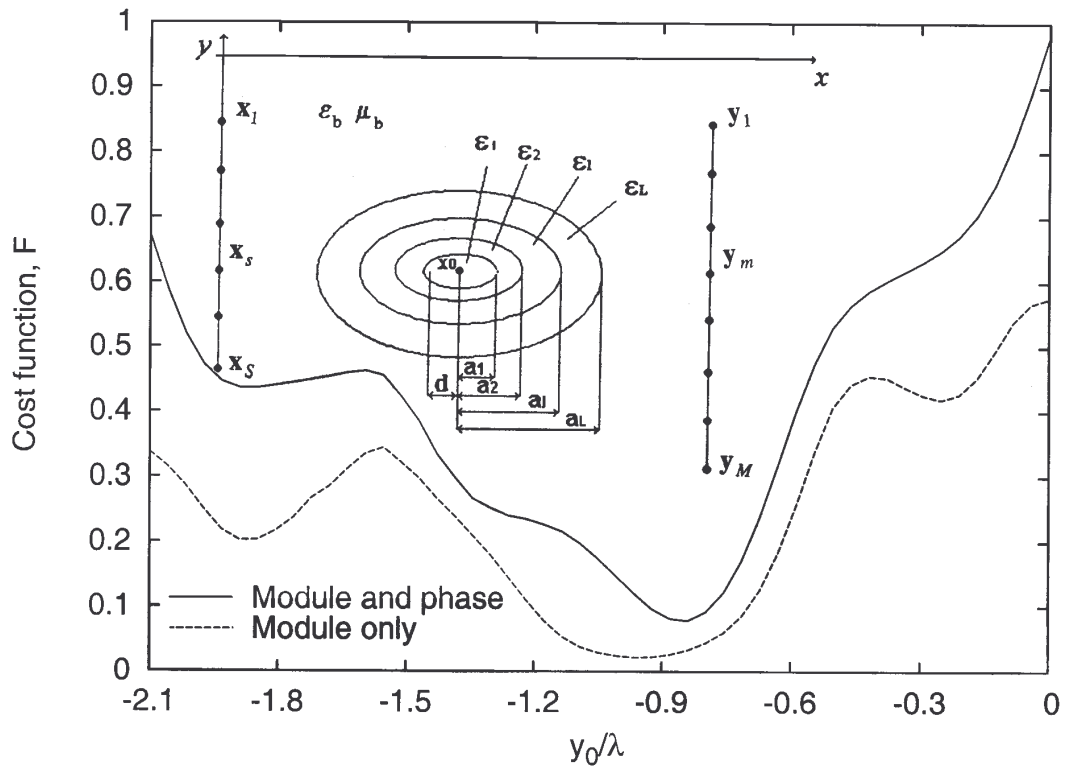
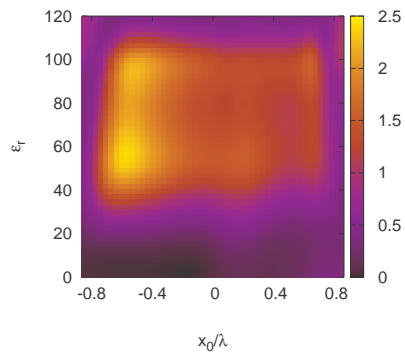
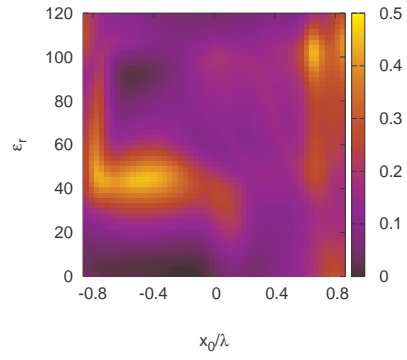


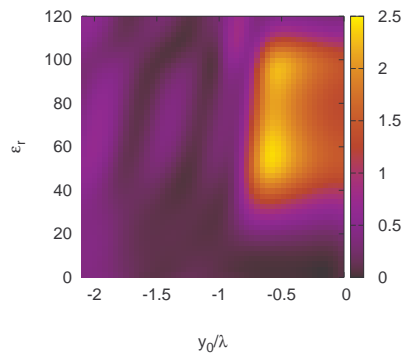
Figure 2



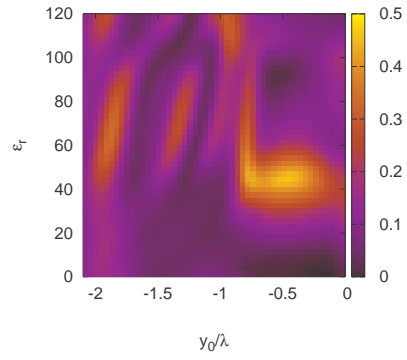
(a)



(b)



(c)



(d)

Figure 3

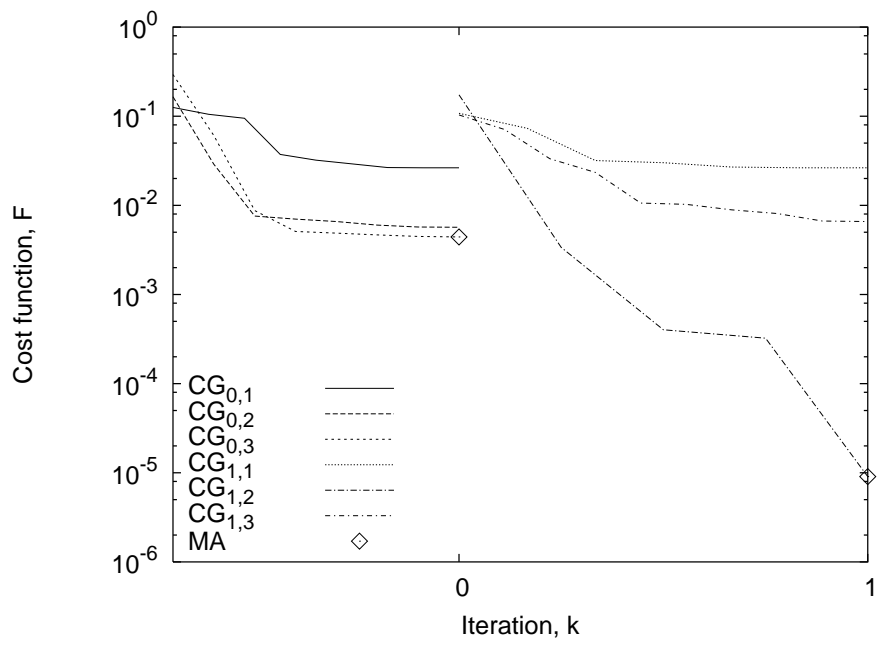


Figure 4

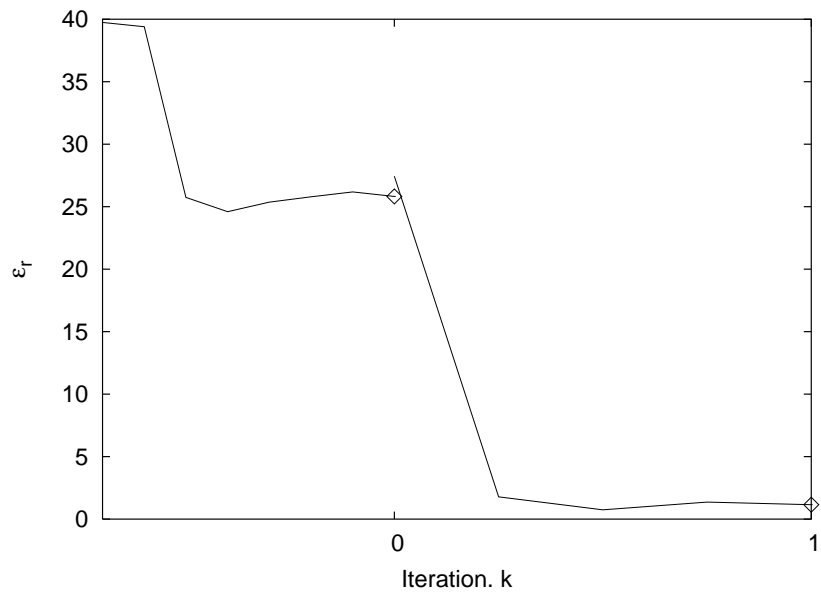


Figure 5

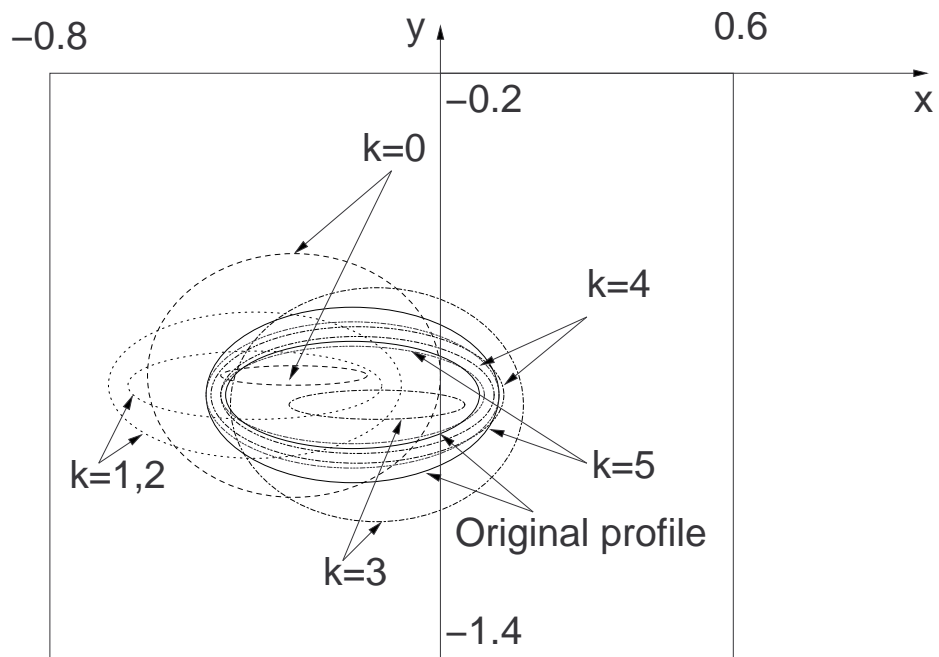


Figure 7

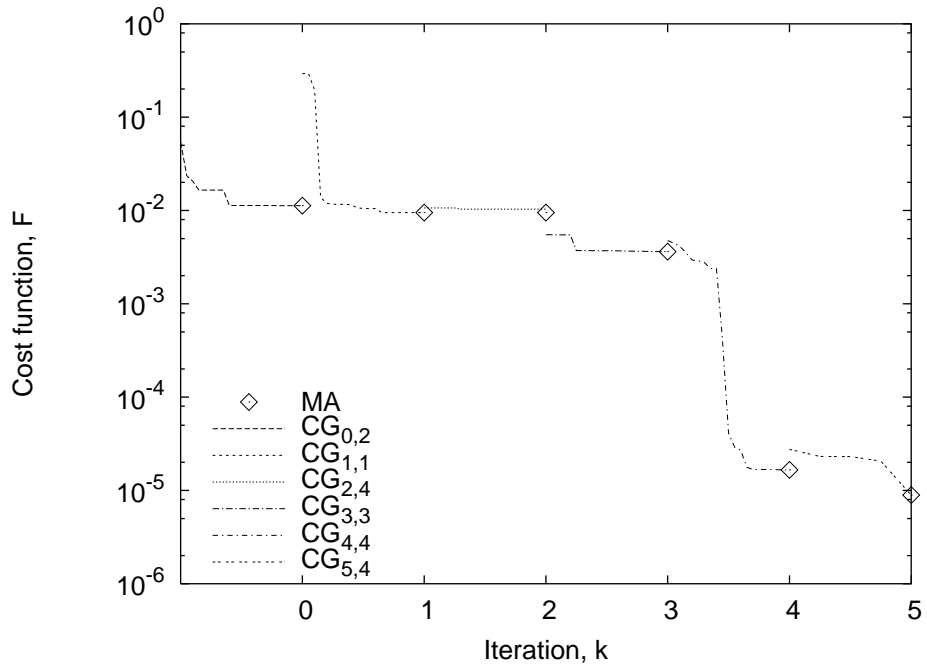


Figure 8

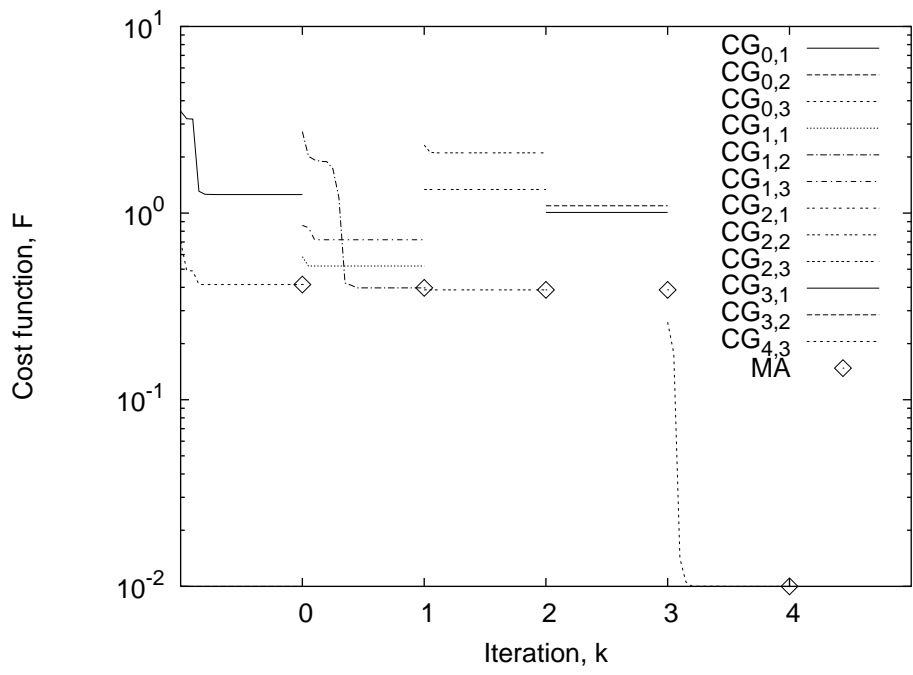


Figure 9

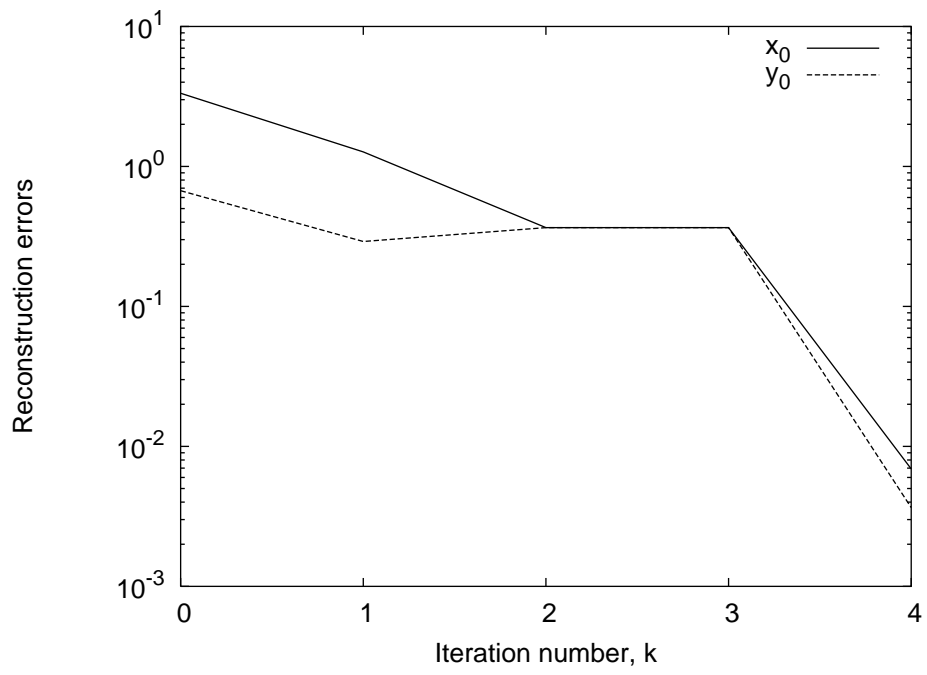


Figure 10

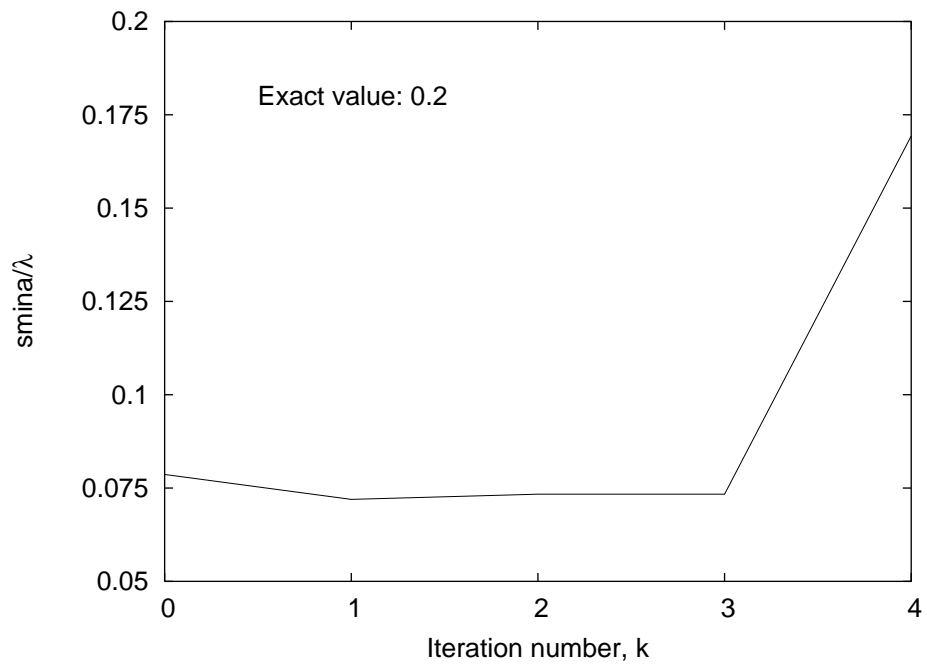
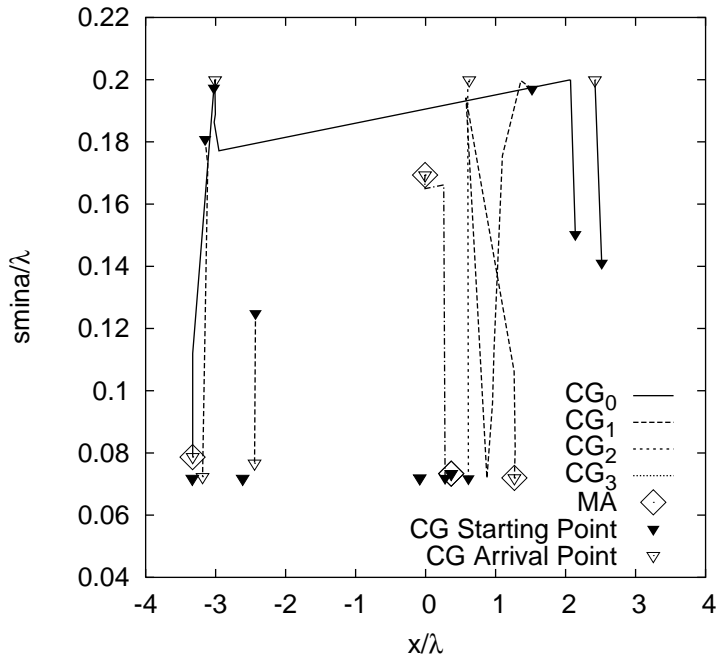
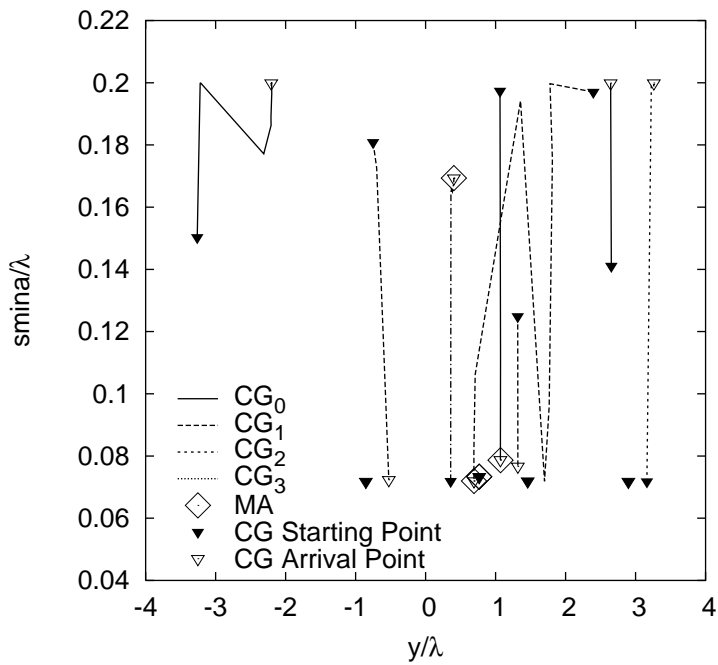


Figure 11



(a)



(b)

Figure 12

<i>Cross-over probability</i>	<i>0.9</i>
<i>Mutation prabability</i>	<i>0.3</i>
<i>Maximun number of iteration for the local search</i>	<i>20</i>
<i>Maximun number of iteration for the memetic algorithm</i>	<i>40</i>
<i>Threshold on $F(\xi_k)$ (local search procedure)</i>	<i>10^{-5}</i>
<i>Threshold on $\ \nabla F(\xi_k)\$ (local search procedure)</i>	<i>10^{-3}</i>
<i>Threshold on $F(\xi_k)$ (memetic algorithm)</i>	<i>10^{-5}</i>
<i>Minimum value of x/λ</i>	<i>-0.865</i>
<i>Minimum value of y/λ</i>	<i>2.1</i>
<i>Minimum value of ε</i>	<i>1.0</i>
<i>Maximum value of x/λ</i>	<i>0.865</i>
<i>Maximum value of y/λ</i>	<i>0</i>
<i>Maximum value of ε</i>	<i>120</i>

Table I